RSC Advances

PAPER

View Article Online
View Journal | View Issue

Cite this: *RSC Adv.*, 2020, **10**, 18959

A porcine acellular dermal matrix induces human fibroblasts to secrete hyaluronic acid by activating JAK2/STAT3 signalling†

Chao Liu and Jiao Sun *

Human facial skin undergoes continuous ageing over a lifespan. At present, facial skin rejuvenation is mainly achieved by injecting filling materials. However, conventional materials lack long-term beneficial effects and can only rejuvenate the skin temporarily by physical filling. To overcome this shortcoming, this study developed a porcine acellular dermal matrix with a porous three-dimensional scaffold structure and containing natural growth factors (3D-GF-PADM). The average size of the 3D-GF-PADM particles was 33.415 μm, and the dynamic viscosity and elastic modulus were within ranges suitable for clinical applications. Our study revealed that the 3D-GF-PADM exhibited an extremely low α-gal epitope number ($3.15 \pm 0.84 \times 10^{11}$/mg) and DNA content, and no immunotoxicity, but contained abundant TGF-β1, VEGF and other growth factors. More importantly, this 3D-GF-PADM actively induced the synthesis of hyaluronic acid by fibroblasts of the host skin. Study at the molecular level further demonstrated that the 3D-GF-PADM activated the JAK2/STAT3 pathway, resulting in the upregulation of HAS2 expression, which led to an increase in hyaluronic acid synthesis. Our study developed a novel 3D-GF-PADM that can actively induce hyaluronic acid synthesis, which may be used clinically as a skin filling material to achieve long-term skin rejuvenation.

Received 18th May 2019
Accepted 26th April 2020

DOI: 10.1039/c9ra03736e

rsc.li/rsc-advances

1. Introduction

A major mechanism underlying skin ageing is the reduction of extracellular matrix components, including collagen and hyaluronic acid.[1] Current treatments mainly use local injections of collagen or hyaluronic acid, which can function effectively as physical fillers for a certain period of time.[2] However, as time elapses, filling materials degrade and the local tissue returns to its original state, suggesting that this type of physical filler based on exogenous injection cannot fundamentally delay the ageing of the skin. Therefore, the bottleneck in this field is how to overcome this temporary filling effect. It has been shown that the structure of the filling material and growth factors affect the production of collagen and hyaluronic acid by the host. Yingjie *et al.* found that a three-dimensional environment for culturing fibroblast-like synoviocytes results in higher HAS2 expression in a triple-layered cell sheet than in the control group.[3] Other groups also found that the addition of certain growth factors, such as TGF-β1, stimulated the production of hyaluronan or collagen.[4,5] Therefore, filling materials with a three-dimensional scaffold structure containing certain growth factors may effectively induce the production of collagen and hyaluronic acid. However, owing to destruction during the production process, the collagen materials currently used in a clinical context lack these growth factors that are abundant in natural collagen. Therefore, a novel biomimetic material with the topography of natural biomaterials and containing the original growth factors that can physically and biologically induce the regeneration of extracellular matrix components, particularly hyaluronic acid, may be able to overcome the temporary effect of current physical fillers.

In recent years, with its three-dimensional structure and growth factors, granular porcine acellular dermal matrix has demonstrated excellent biological activity and has become of interest to researchers. Zhou *et al.* used granular porcine acellular dermal matrix as a carrier to deliver adipose tissue-derived mesenchymal stem cells, which then upregulated the expression of bone formation-related genes.[6] In addition, Xiaojun *et al.* found that fibroblasts infiltrated into the granular porcine acellular matrix were highly proliferative.[7] However, it remains to be seen whether granular porcine acellular matrix could be used as dermal filler. Based on the above-mentioned findings, we speculated that, with its porous three-dimensional network structure and large amount of growth factors, granular porcine acellular matrix could effectively induce hyaluronic acid synthesis by skin fibroblasts. This granular porcine acellular matrix will likely demonstrate better efficacy than current physical fillers, thereby benefiting patients and advancing the field of skin injection and filling.

Shanghai Ninth People's Hospital, Shanghai Jiaotong University School of Medicine, Shanghai Biomaterials Research and Testing Center, Shanghai 200023, China. E-mail: jiaosun59@shsmu.edu.cn; Tel: +86-21-63034903

† Electronic supplementary information (ESI) available. See DOI: 10.1039/c9ra03736e

In this study, we developed a granular porcine acellular dermal matrix (3D-GF-PADM) with a porous three-dimensional scaffold structure and containing growth factors, and characterised it, including its molecular weight, amino acid composition, particle size distribution, dynamic viscosity, growth factor content, and immunogenicity. We then examined the effect of this 3D-GF-PADM on the secretion of hyaluronic acid from human skin fibroblasts, and on the expression of genes involved in hyaluronic acid secretion. We finally investigated the role of JAK2/STAT3 signalling in the process of 3D-GF-PADM-induced hyaluronic acid secretion. In summary, this study developed a novel 3D-GF-PADM and evaluated its biological activity on fibroblasts; our data provide a scientific basis for using this novel 3D-GF-PADM as a skin cosmetic filling material.

2. Materials and methods

2.1. Preparation of 3D-GF-PADM

3D-GF-PADM was provided by Jiangsu Unitrump BioMedical Technology Co., Ltd. (Nanjing, China). It was prepared as follows: skin was removed from healthy white piglets (~50 kg), shaved and washed, a 0.3–0.5 mm-thick skin patch was made on a leather machine and cut into pieces of 4 × 5 cm in size. These pieces were then disinfected with chlorhexidine solution and immersed in hypertonic saline for 24 h. The epidermis was peeled off gently and decellularised with reagents mainly composed of trypsin after crosslinking with glutaraldehyde; then, the decellularised epidermis was rinsed with saline and lyophilised. For the production of ultrafine powder, an ultrafine grinding technique was used.

2.2. Assessment of α-gal in 3D-GF-PADM

To qualitatively examine the content of α-gal epitopes in acellular dermal matrix, the acellular dermal matrix sheet was sectioned with a freezing microtome and then mounted onto poly-L-lysine-coated (PLL-coated) glass slides. After being fixed with pre-cold acetone for 5 min, cryo-sections were incubated in 3% H_2O_2 at room temperature for 10 min. Then the cryo-sections were incubated in 3% (w/v) BSA/PBS (pH 7.4) at room temperature for 30 min. And then FITC-conjugated Isolectin B4 (BSI-B4, Sigma, St. Louis, MO, USA) in 3% BSA/PBS (dilution 1 : 100) was applied at 37 °C for 3 h. Original porcine skin used as a positive control. All the experiments were repeated independently three times.

For quantitative measurement of α-gal, 3D-GF-PADM (60 mg) and porcine skin (60 mg) were added into separate sterile 1.5 ml centrifuge tubes. Then, 1 ml of RIPA buffer containing PMSF was added to each tube, after which the tubes were shaken once every 10 min for 30 min and then centrifuged at 13 000*g* for 10 min, followed by collection of the supernatants. SP2/0 cells were obtained from the cell bank of the Chinese Academy of Sciences and cultured in high-glucose DMEM medium at 37 °C. A solid-phase antigen-coated plate was prepared by using 2 μg ml^{-1} Galα1-3gal-BSA (NGP0203, Dextra, 500 μg ml^{-1} Gal/BSA) that diluted with PBS. Then, 100 μl of M86 antibody (ALX-801-090-1, Enzo, M86 antibody diluted with PBS at 1 : 50) was applied to the SP2/0 cells and incubated at 4 °C overnight. Following centrifugation at 13 000*g* for 10 min at 4 °C, the supernatant was collected, transferred into solid-phase antigen-coated plates, and incubated at 4 °C overnight. Then, after incubation with 100 μl of rabbit anti-mouse secondary antibody (ab186701; Abcam) at 37 °C for 1 h, the absorbance at 450 nm was read.

2.3. Determination of residual DNA content in 3D-GF-PADM

3D-GF-PADM porcine skin was cut into small pieces, which were digested with proteinase K solution at 37 °C on a shaker overnight, and then centrifuged at 13 000*g* for 30 min. Phenol–chloroform–isoamyl alcohol was added to the supernatant, followed by centrifugation again at 13 000*g* for 30 min. Discarding the aqueous layers and adding ethanol to precipitate the DNA, DNA concentration was measured using the Quant-iT™ PicoGreen dsDNA reagent (Thermo Fisher Scientific, USA, P7581) following the manufacturer's instructions.

2.4. Morphological examination

The 3D-GF-PADM surface and morphology were examined by scanning electron microscopy (SEM).

2.5. Determining the molecular weight of 3D-GF-PADM

The molecular weight of 3D-GF-PADM was measured by AXIMA Performance MALDI-TOF/TOFMS. α-Cyano-4-hydroxycinnamic acid was used as the matrix and the 3D-GF-PADM sample (1 mg ml^{-1}) was dissolved in water. A total of 0.5 μl of the 3D-GF-PADM solution was mixed with 0.5 μl of the matrix solution, after which the mixture was added to the MALDI plate. The molecular weight of 3D-GF-PADM was measured by the machine and the data were analysed by Data Explorer 4.0.

2.6. Measurement of particle size

The particle size of the 3D-GF-PADM was measured using a Malvern laser particle size analyser (Malvern Instruments, Malvern, UK). 3D-GF-PADM samples were placed in suspension in water and scanned for mean particle size and distribution in the particle analyser.

2.7. Measurement of dynamic viscosity and elastic modulus

The dynamic viscosity and elastic modulus of 3D-GF-PADM were measured using a Haake MARS rheometer (Thermo Scientific, Karlsruhe, Germany). The distance between the two vertical plates of the viscometer was set to 1 mm, and the shear rate range used was 0.1–2.0 Hz. The elastic modulus was measured at 1 Hz and 23 °C.

2.8. Determination of amino acid content of 3D-GF-PADM

Two milligrams of 3D-GF-PADM was added to a hydrolysis tube, to which 4 ml of 6 N HCl was also added, followed by filling with nitrogen for 6 min and sealing. The tube was incubated for 24 h at 110 °C and the amino acid content was analysed using a Hitachi L-8900 High Speed Amino Acid Analyzer. The content of amino acid was expressed as the number of residues per 1000 amino acids.

2.9. Measurement of retained cytokines

ELISA was used to quantify the retained cytokines in 3D-GF-PADM. Cytokines were extracted using commercial lysis buffer for total protein extraction from 3D-GF-PADM and original porcine skin (FNN0071; Thermo Fisher Scientific). The extracted material was centrifuged at 10 000*g* for 10 min and then the supernatant was separated. The protein concentration was determined by Bradford assay. The following ELISA kits were used: basic fibroblast growth factor (bFGF) (E-EL-P0744; Elabscience), transforming growth factor beta1 (TGF-β1) (MB100B; R&D Systems), vascular endothelial growth factor (VEGF) (LS-F5749; LifeSpan Biosciences) and Platelet Derived Growth Factor-BB (PDGF-BB) (ELP-PDGFB; RayBiotech, Inc.).

2.10. *In vitro* degradation

The stability of 3D-GF-PADM against enzymatic degradation was assessed through exposure to collagenase *in vitro*. Freeze-dried 3D-GF-PADM was weighed (W_1) and incubated in 1.5 ml of 100 mg ml^{-1} collagenase type I (Sigma-Aldrich, St. Louis, MO) at 37 °C. On days 1, 2, 4 and 7, the digested suspension was centrifuged at 5000*g* for 5 min. The supernatants were discarded and the remaining sediments were dried at 37 °C for 12 h in a vacuum oven. Subsequently, the dried digested specimens were weighed (W_2). The proportion of the mass of 3D-GF-PADM remaining after enzymatic digestion was calculated using the following formula: $W_2/W_1 \times 100$. All tests were performed in triplicate.

2.11. $CD4^+/CD8^+$ ratio determination

This study was approved by the Ethics Committee of Shanghai Ninth People's Hospital, affiliated with the School of Medicine, Shanghai Jiao Tong University. 3D-GF-PADM was implanted subcutaneously into mice (BABL/c, 1 g per kg) for 1 month. $CD4^+$ and $CD8^+$ cells in the blood were detected by flow cytometry, and the level of IgG/IgM in the blood was detected by an IgG ELISA kit (88-50400-88; eBioscience) and IgM ELISA kit (88-50470; eBioscience).

2.12. Skin irritation and skin sensitisation test

The experiment was approved by the Ethics Committee of Shanghai Ninth People's Hospital, affiliated with the School of Medicine, Shanghai Jiao Tong University. New Zealand White rabbits with body weight ranging from 2.5 to 3.2 kg were used. A total of 0.5 ml or 1 ml of 3D-GF-PADM with or without lidocaine (1% and 2%) and the same amount of control sample (0.9% NaCl) were injected intracutaneously into three separate sites on the shaved area of the back of each rabbit. Then, macroscopic assessments of oedema and erythema at the injection sites were carried out using a 0–4 grading scale (ESI Table 1†) immediately after injection, as well as 24, 48, and 72 h later.

For the skin sensitisation test, male guinea pigs (6 weeks old) were utilized for both the 3D-GF-PADM group and the NaCl group. An intradermal induction phase, topical induction phase, and challenge phase were included in this test. Both 3D-GF-PADM (0.5 ml or 1 ml with or without 1% or 2% lidocaine) and NaCl were intradermally injected and applied with an occlusive patch to the experimental animals; following a break of 14 days (a recovery period), all animals in both 3D-GF-PADM and NaCl groups were then challenged with the corresponding samples. All challenge sites were scored and the skin reactions regarding swelling and erythema were evaluated (0–3 scale; ESI Table 3†) at 24 and 48 h after patch removal.

2.13. Cell culture

Human skin fibroblasts (HSFs) were obtained from the Kunming Cell Bank of the Chinese Academy of Sciences (Kunming, China). HaCaT keratinocytes and B16-F10 melanocytes were purchased from the Cell Bank of the Chinese Academy of Science (Shanghai, China). All of these cells were maintained in DMEM containing 10% fetal bovine serum and passaged at 90% confluence.

2.14. MTT test

HSFs, keratinocytes, and melanocytes were cultured in a 96-well plate and treated with the designated concentrations of 3D-GF-PADM for 24 h. MTT assay was carried out to study the effect of 3D-GF-PADM on the proliferation of HSFs, keratinocytes, and melanocytes.

2.15. DAPI staining

The effect of 3D-GF-PADM on the proliferation of HSFs was observed by fluorescence microscopy. HSFs were added into 96-well plates and treated with 3D-GF-PADM at 1 mg ml^{-1} for 24 h. After washing with PBS three times, the cells were fixed with 4% paraformaldehyde for 30 min and incubated in DAPI solution for 2 min. After washing with PBS three times, the cells were observed under a confocal microscope.

2.16. Detection of type I collagen secretion and hyaluronic acid secretion

HSFs were seeded on 24-well plates and treated with 3D-GF-PADM at 1 or 0.5 mg ml^{-1} for 24 h. Supernatants were then collected and the concentration of type I procollagen carboxy-telopeptide in the supernatant was measured using an ELISA kit (MK101; Takara Bio, Mountain View, CA, USA), following the manufacturer's instructions. The concentration of hyaluronic acid in the supernatant was measured using Hyaluronan Duo-Set ELISA kit (DY3614-05; R&D Systems, USA), in accordance with the manufacturer's manual.

2.17. Real-time polymerase chain reaction (PCR)

HSFs and HaCaT keratinocytes were cultured in a six-well plate and treated with 3D-GF-PADM at 1 or 0.5 mg ml^{-1} for 24 h. The expression level of hyaluronan-related genes including HAS1, HAS2 and HAS3 and collagen synthesis-related gene COL I for HSFs, as well as the MMP-9 gene for keratinocytes, was detected by real-time PCR. The results were normalised based on the gene expression levels in the blank control group. The primers used for real-time PCR are listed in Table 2.

2.18. Melanin content assay

Melanocytes were plated into six-well plates at a density of 1×10^5 cells per well and were incubated for 24 h, followed by treatment with 1 or 0.5 mg ml^{-1} 3D-GF-PADM for 48 h. Then, the cells were washed three times with pre-chilled PBS and collected by trypsinisation. After centrifugation, the cells were dissolved in 100 μL of 1 M NaOH at 80 °C for 1 h and then centrifuged at 13 000 × *g* for 10 min. The supernatants were transferred into a 96-well microplate, followed by measurement of the relative melanin content at 405 nm with a microplate reader. The relative melanin content in 3D-GF-PADM-treated cells was expressed as the percentage relative to the control (untreated melanocytes).

2.19. Western blot

HSFs were cultured in 100 mm Petri dishes. The inhibitor group was first treated with the small-molecule inhibitors SB431542, LY294002, AG490 or PD98059 for 2 h (10 μM). The inhibitors SB203583 (a p38 inhibitor), SP600125 (a JNK inhibitor), U0126 (an ERK1/2 inhibitor), AG490 (a JAK inhibitor) and BX795 (a TBK1 inhibitor) were purchased from Millipore (Billerica, MA). Then, the cells were treated with 3D-GF-PADM at 1 mg ml^{-1} for 24 h. After collection, total protein extraction was done with RIPA buffer containing phosphatase and protease inhibitors (Pierce, Rockford, IL, USA). After separation using a 12% SDS-PAGE denaturing gel and transfer to PVDF membranes, the membranes were blocked with 5% skim milk. The primary antibodies, including JAK2 (Abcam; ab108596), p-JAK2 (Abcam; ab32101), STAT3 (Abcam; ab68153), p-STAT3 (Abcam; ab76315) and HAS2 (Abcam; ab140671), were used at 4 °C overnight. Secondary antibody incubation was performed at room temperature for 1 h.

2.20. Confocal microscopy

HSFs were seeded on coverslips. The inhibitor group was first treated with AG490 at a final concentration of 10 μM for 2 h, and then with 3D-GF-PADM at 1 mg ml^{-1} for 24 h. Cells were washed with PBS three times, fixed with 4% paraformaldehyde for 30 min and washed three times with PBS. Cells were permeabilised in PBS containing 0.5% Triton X-100 (PBST) for 10 min at room temperature, washed with PBS three times, blocked with PBST containing 1% bovine serum albumin at room temperature for 1 h and incubated with HAS2 primary antibody (diluted 1 : 200 in blocking buffer) at 4 °C overnight. Cells were rinsed with PBS three times, incubated with Alexa Fluor® 488-conjugated secondary antibody in the dark for 1 h at 37 °C and rinsed with PBS 3 times. Cells were then incubated with phalloidin at 37 °C for 1 h in the dark, washed with PBS three times, counterstained with DAPI for 2 min and rinsed with PBS three times. Coverslips were mounted and observed under a confocal microscope.

2.21. *In vivo* study

The experiment was approved by the Ethics Committee of Shanghai Ninth People's Hospital, affiliated with the School of Medicine, Shanghai Jiao Tong University. Healthy male white rabbits, weighing 2.5–3.0 kg, were used in this study. The injection site on each ear was shaved and then 1 ml of 3D-GF-PADM at a concentration of 195 mg ml^{-1} (prepared in saline, containing 1% lidocaine) was injected into the dorsal dermis of the ear. Groups of rabbits ($n = 3$ per group) were sacrificed at day 7, 1 month and 3 months. The injection sites and surrounding tissues were collected and fixed in formalin, dehydrated and embedded in paraffin following standard histological protocols. Haematoxylin and eosin (H&E) staining was performed to examine the host response at the injection site. Normal rabbits without injection were set as a control group.

2.22. Data analysis

Data collected from at least three independent experiments were expressed as mean ± standard deviation. SPSS11.0 software was used to perform statistical analysis to examine whether there was a statistically significant difference between groups ($P < 0.05$).

3. Results and discussion

The three-dimensional structure and growth factor components are important physical and chemical factors that affect the function of implanted biological materials. Previous studies found that certain three-dimensional morphology induces the generation of mechanical stimulating signals, which then induces cell differentiation and activates signal transduction.[8] In addition, growth factors play various roles in mediating the biological functions of cells.[9,10] The 3D-GF-PADM used in this study exhibits a unique three-dimensional structure and contains certain growth factors. However, it remained unclear how this 3D-GF-PADM might affect the function of skin fibroblasts. Because hyaluronic acid and collagen have been extensively used for skin anti-ageing applications, it is of great interest to scientists and clinicians in the skincare field to study whether this 3D-GF-PADM interacts with host skin fibroblasts and mediates the production of hyaluronic acid and collagen. In the present study, by improving the production process, we developed a novel 3D-GF-PADM with a modified three-dimensional structure and containing certain growth factor; our results showed that it actively induced the production of hyaluronan.

3.1. 3D-GF-PADM exhibits a complete, porous three-dimensional network and properties suitable for use as physical filler

The ideal skin filling material should exhibit a suitable structure to achieve a relatively long subcutaneous residence time and enable easy injection. The 3D-GF-PADM fabricated by mechanical pulverisation in this study preserves the fibrous structure of the native collagen. As shown in Fig. 1A and B, this 3D-GF-PADM exhibits a complete three-dimensional network structure and shows large pores between fibres, which result in a large specific surface area. Previous studies suggested that larger pores in the collagen matrix promote the diffusion of

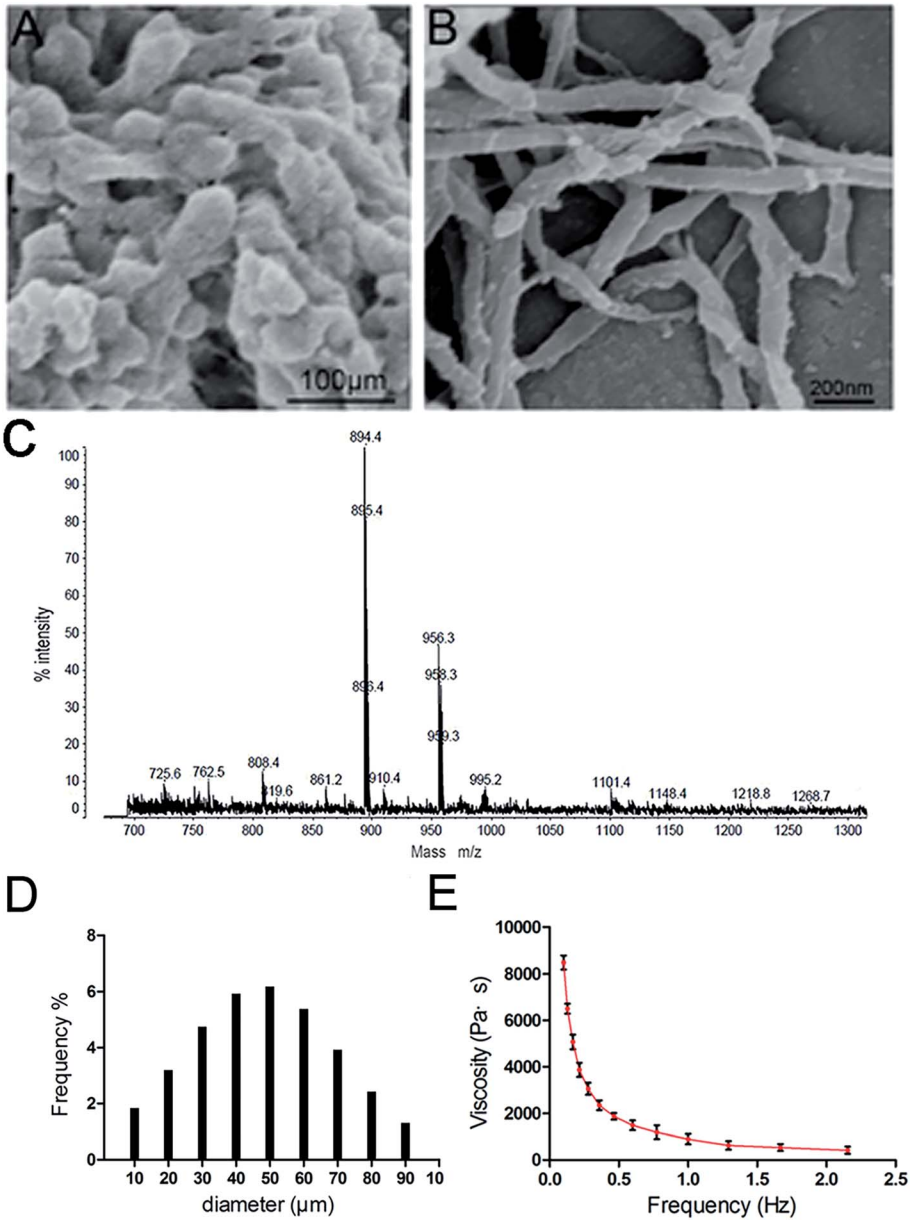

Fig. 1 (A and B) Representative scanning electron microscopy (SEM) images of the 3D-GF-PADM demonstrate the 3D crossed fibroid structure. Scale bars: (A) 100 μm; (B) 200 nm. (C) A low and narrow distribution of molecular weight of 3D-GF-PADM. (D) The particle size distribution of 3D-GF-PADM. The mean diameter was 50 μm. (E) The dynamic viscosity of 3D-GF-PADM decreased with increasing frequency.

nutrients and removal of waste, thereby effectively promoting the adhesion and early-stage proliferation of cells.[11] Therefore, it can be speculated that the structure of this 3D-GF-PADM is probably conducive to the penetration, adhesion and proliferation of fibroblasts *in vivo*.

The size of particles also affects the function of filling materials. The average particle size of the 3D-GF-PADM is 33.415 μm (Fig. 1D). These small particles can easily pass through a syringe needle, making their clinical application feasible.[12] Apart from being smaller, the particles' size is also uniform and narrowly distributed. This uniform size is helpful for the accurate injection of particles because it is less likely that plastic surgeons will experience inconsistent resistance during injection. In addition, dynamic viscosity and elastic modulus are important parameters for assessing the resistance of filler materials to deformation and movement. We found that the 3D-GF-PADM exhibits the characteristics of a pseudoplastic body (shear thinning), that is, it has a higher viscosity under low shear rate conditions and its viscosity decreases with increasing shear rate (Fig. 1E). The shear rate of the 3D-GF-PADM is low after injection into the dermis, and then the high viscosity can reduce the movement of the filler underneath the skin. By contrast, the shear rate is high when the filler is being pushed out from the syringe. During this process, the viscosity of the filler is drastically reduced with increasing shear rate, and therefore it is easy to inject the filler from the needle, which

allows doctors to precisely control the injection process and increases patients' comfort.

The proportions of the mass of 3D-GF-PADM remaining after different digestion times are shown in ESI Fig. 1.† The residual proportion of the mass of 3D-GF-PADM showed only minimal change with increasing enzymatic digestion time. After 7 days of exposure to collagenase, there was still 81.7 ± 4.8% remaining in the 3D-GF-PADM group. In the present study, 3D-GF-PADM showed prolonged endurance in the presence of collagenase. Collagenase activity depends on its concentration, but the concentration used in this study was much higher than that *in vivo*.[13,14] Although this *in vitro* experimental set-up may thus not closely simulate the physiological environment *in vivo*, it is adequate to demonstrate the resistance to enzymatic degradation, which is an important characteristic of skin fillers. Taken together, the physical characteristics suggest that the 3D-GF-PADM is an excellent candidate skin filling material for clinical injections.

3.2. 3D-GF-PADM has low immunogenicity

The biosafety of xenogenic biomaterials must be examined before clinical application. It has been suggested that specific natural IgG antibodies react with α-gal antigens, which raises concerns about the immunogenicity of mammalian-derived biomaterials.[15] Further work has confirmed that the expression of α-gal antigen on the surface of xenografts is the key factor that causes hyperacute immune rejection and chronic immunotoxicity.[16]

Because the 3D-GF-PADM material in this study was derived from porcine skin, we were concerned about whether the decellularisation process affected its α-gal content. Specific binding of isolectin B4 showed strong bands in the control, but not in the 3D-GF-PADM (Fig. 2A and B). The number of antigenic epitopes in the 3D-GF-PADM and porcine skin is 3.15 ± 0.84 × 10^{11}/mg and 6.55 ± 1.80 × 10^{11}/mg, respectively (Fig. 2C). The number of antigenic epitopes was thus reduced by approximately half in the former, suggesting that the 3D-GF-PADM has lower immunotoxicity. In addition, the content of residual DNA in the 3D-GF-PADM was significantly lower than that in the original porcine skin (Fig. 2D).

To examine the immunogenicity of the 3D-GF-PADM, it was implanted subcutaneously into BALB/c mice. We found that the $CD4^+/CD8^+$ ratio in the implantation group was lower than that in the control group (injected with PBS). Previous studies showed that the $CD4^+/CD8^+$ ratio normally ranges from 1 to 4, and a higher $CD4^+/CD8^+$ ratio may be indicative of higher systemic immune reaction,[17] suggesting that the 3D-GF-PADM did not induce a strong immune response (Fig. 3A). In addition, the levels of IgG and IgM in the experimental group were similar to those in the control group (injected with PBS) (Fig. 3B). Taken together, these findings suggest that the 3D-GF-PADM demonstrates a tolerable *in vivo* safety profile with no significant immunogenicity. Here, it is worth noting that mice are the most frequently used animal model, especially in the research area of physiology and biochemistry, since they are cheap and easy to handle and maintain, and reproduce rapidly.

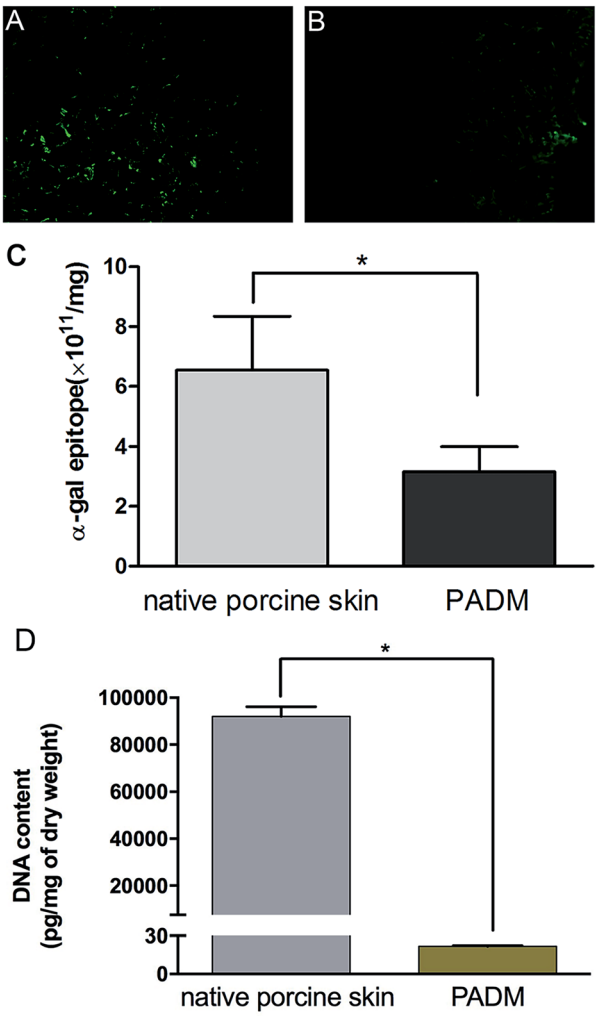

Fig. 2 (A and B) There was high α-gal epitope expression in the native porcine skin (A), but this epitope was minimally present in the 3D-GF-PADM (B) assessed by FITC-conjugated Isolectin B4 staining. (C) Quantification of α-gal epitope in 3D-GF-PADM showed the significantly lower content than that in the native porcine skin. (D) Quantification of residual DNA content showed the significantly lower content in 3D-GF-PADM than that in the native porcine skin.

However, mice have many physiological differences from humans. They thus do not effectively replicate the entire pathogenesis of specific human diseases. It is hard to bridge this gap between mice and human patients, so in the context of this

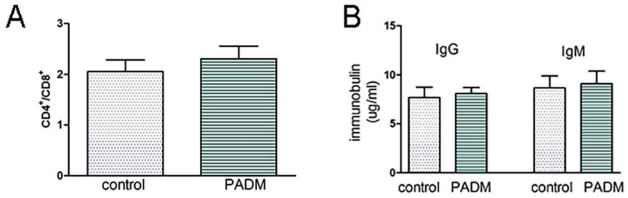

Fig. 3 Evaluation of the immunogenicity of 3D-GF-PADM. (A) The ratio of $CD4^+/CD8^+$. (B) 3D-GF-PADM did not stimulate the secretion of IgG and IgM.

work, studies in human participants are required to characterise the immunotoxicity of 3D-GF-PADM.

Skin irritation characterised by oedema and erythema was scored based on the scoring system (ESI Table 1†). All scores for the 3D-GF-PADM groups were 0, suggesting that they exhibited no oedema or erythema. Moreover, all study animals were found to be clinically normal, and there were no significant differences between 0.5 ml and 1 ml 3D-GF-PADM, suggesting there was no dose related response (ESI Table 2†). Thus, 3D-GF-PADM can be considered as a non-irritant. Skin sensitisation is an immune response to previous exposure to a chemical that results in an inflammatory skin reaction. In the present study, at 24 and 48 h after the challenge phase, the score in each animal in the 3D-GF-PADM group was 0 (ESI Tables 3 and 4†). There was no visible allergic response in all skin sites of experimental animals in the 3D-GF-PADM group. And there was no dose–response relationship between 3D-GF-PADM and the skin reaction as shown in ESI Table 4,† there were no significant differences between 0.5 ml and 1 ml 3D-GF-PADM. This suggests that 3D-GF-PADM is not a skin-sensitising substance, so one may reasonably extrapolate that the associated risk of allergic skin reaction in humans would be negligible. In addition, lidocaine is a local anaesthetic medication that has been subcutaneously used in cosmetic surgery, the administration of lidocaine can effectively decrease the occurrence of pain and discomfort during the procedure.[18] In the present study, the addition of lidocaine to 3D-GF-PADM did not evoke any side effects, there is no difference between the group with lidocaine and the group without lidocaine in terms of oedema, erythema, swelling or bruising (ESI Tables 5 and 6†), which indicate that mixing of lidocaine into the 3D-GF-PADM did not compromise its performance.

3.3. 3D-GF-PADM contains abundant growth factors

In addition to the three-dimensional structure, growth factors are also essential for promoting the production of hyaluronan. Myung *et al.* found that certain growth factors such as bFGF could increase the mRNA level of HAS2.[19] In the present study, we found that the 3D-GF-PADM contains abundant growth factors including TGF-β1, VEGF, bFGF and PDGF-BB (Fig. 4). It has been found that TGF-β1 and VEGF can promote cell proliferation, as can bFGF and PDGF-BB.[20] bFGF and PDGF-BB are effective inducers of hyaluronic acid production. These results indicate that 3D-GF-PADM may have good biological behaviour. With regard to explaining the presence of growth factors in 3D-GF-PADM, these are present because the extracellular matrix

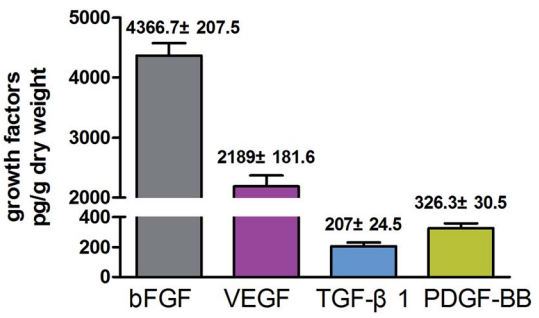

Fig. 4 ELISA was used to quantify the retained cytokines in 3D-GF-PADM. The following ELISA kits were used: basic fibroblast growth factor (bFGF) (E-EL-P0744; Elabscience), transforming growth factor beta1 (TGF-β1) (MB100B; R&D Systems), vascular endothelial growth factor (VEGF) (LS-F5749; LifeSpan Biosciences) and Platelet Derived Growth Factor-BB (PDGF-BB) (ELP-PDGFB; RayBiotech Inc.).

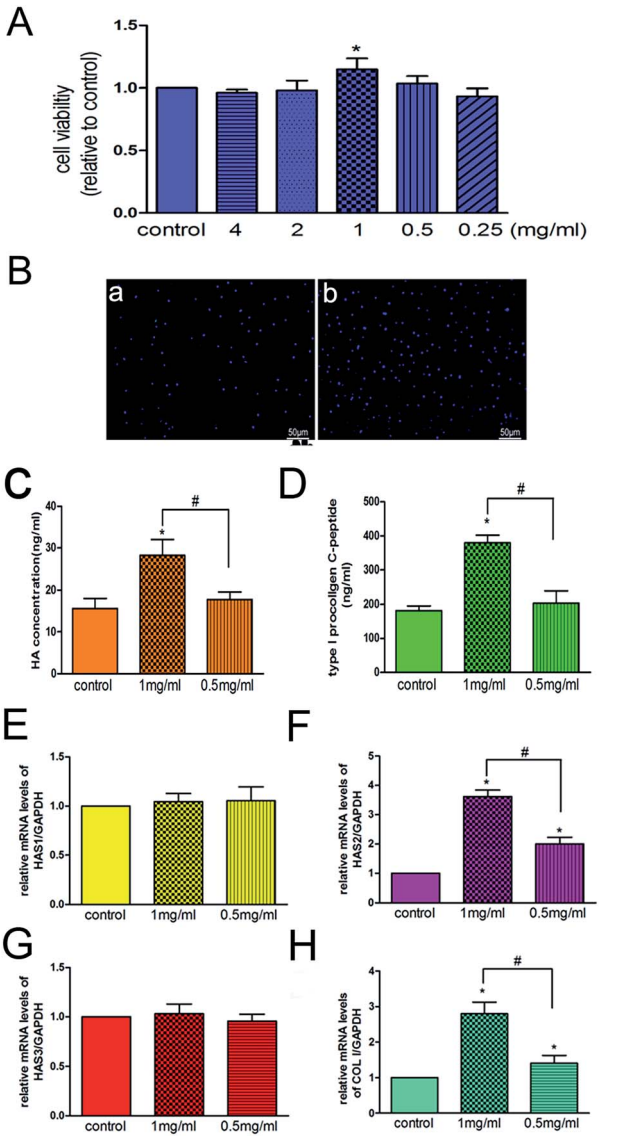

Fig. 5 (A) HSFs were treated with various concentrations of 3D-GF-PADM. MTT results showed that 1 mg ml^{-1} 3D-GF-PADM enhanced the proliferation of HSFs. (B) 4,6-Diamidino-2-phenylindole (DAPI) staining was used to analyse the effect of 3D-GF-PADM treatment on cell viability. A significant difference was observed between the 3D-GF-PADM treatment group and the control group. (C) The increased HA secretion induced by 1 mg ml^{-1} 3D-GF-PADM. (D) The increased collagen secretion induced by 1 mg ml^{-1} 3D-GF-PADM. (E) The relative HAS1 mRNA expression after treatment with 3D-GF-PADM. There was no significant change compared with the control group. (F) The relative HAS2 mRNA expression after treatment with 3D-GF-PADM. After treatment with 1 mg ml^{-1} 3D-GF-PADM, the expression of HAS2 was increased. (G) The relative increase of HAS3 mRNA expression after treatment with 3D-GF-PADM. (H) The relative COL I mRNA expression after treatment with 3D-GF-PADM.

Table 1 Determination of amino acids of 3D-GF-PADM

Amino acid	PADM residues/1000
Ala	114
Arg	51
Asp	46
Cys	2
Glu	76
Gly	335
His	3
Hyp	92
Ile	10
Leu	24
Lys	24
Phe	13
Pro	135
Ser	33
Thr	17
Tyr	2
Val	23
Total	1000

(ECM) is a highly complex meshwork of signalling factors and insoluble fibrillar proteins interacting together to provide mechanical and chemical cues to maintain tissue architecture and homeostasis.[21] It is well established that the ECM acts as a reservoir for several growth factors and signalling molecules.[22,23] Generally, growth factors are secreted by cells and then bind in the ECM; for example, fibronectin domains of ECM have been found to bind to VEGF and HGF.[24,25] Moreover, heparin sulphate proteoglycans, which are abundant in the ECM, have been found to bind FGFs and sequester them for storage.[26] Decellularised ECM is similar to the original ECM in terms of composition and structure. Decellularised ECM from many organs or tissues is able to retain some growth factors after the entire decellularisation process.[27–32] In the present study, as ECM-based biomaterials, we can reasonably speculate that these growth factors bind to specific components in the 3D-GF-PADM. However, the underlying binding sites and binding mechanism still need further investigation.

3.4. 3D-GF-PADM promotes the secretion of collagen and hyaluronic acid from skin fibroblasts, while having no effects on keratinocytes and melanocytes

Because decreased proliferative capacity of skin fibroblasts is one of the most important factors contributing to skin ageing,[33] one strategy adopted for treating skin ageing is to promote the proliferation of fibroblasts. We found that 3D-GF-PADM at 1 mg ml^{-1} effectively promoted the proliferation of HSFs ($P < 0.05$) (Fig. 5A), which is consistent with the DAPI staining results (Fig. 5B). The proliferation of HSFs may be induced by extracellular matrix components in the acellular dermal matrix, such as type I and III collagen, which provides multiple binding sites to facilitate HSFs adhesion and proliferation.[34,35]

The reduction of collagen and hyaluronic acid secreted by skin fibroblasts also contributes to skin ageing. In this study, we found that 3D-GF-PADM at 1 mg ml^{-1} actively induced the secretion of hyaluronic acid by fibroblasts (Fig. 5C), which may render 3D-GF-PADM superior to conventional skin filling materials. The secretion of hyaluronic acid by fibroblasts may be induced by multiple factors in the 3D-GF-PADM: (1) the specific amino acid composition, as the 3D-GF-PADM contains large amounts of proline (135/1000) and hydroxyproline (92/1000) (Table 1), which can promote hyaluronan synthesis by HSFs,[36] and (2) bFGF and PDGF-BB (Fig. 4), which can induce the production of hyaluronic acid by fibroblasts.[37]

Keratinocytes are the predominant cells in the epidermis, constituting approximately 95% of epidermal cells, and play an important role in maintaining epidermal homeostasis.[38] In the present study, there was no difference in the viability of keratinocytes when cells were compared between the 3D-GF-PADM and control groups (ESI Fig. 2A†). MMP-9 has been shown to be expressed in keratinocytes and involved in enhancing their migration.[39] In the present study, the mRNA level of MMP-9 showed no difference between the 3D-GF-PADM and control groups (ESI Fig. 2B†). This suggests that the 3D-GF-PADM did not have a significant effect on the viability and function of keratinocytes.

In addition, melanocytes are an important cell type in the skin's epidermis through their functioning in melanin production.[40] In the current study, no significant differences were found in cell viability between the 3D-GF-PADM and control groups (ESI Fig. 3A†). Melanin is the major determinant of skin colour in humans. Compared with that in the control group, melanin production in the 3D-GF-PADM group showed no statistically significant difference (ESI Fig. 3B†).

Next, we investigated the molecular mechanism by which 3D-GF-PADM induces the production of hyaluronic acid. In humans, three genes, HAS1, HAS2 and HAS3, encode hyaluronic acid synthases and are expressed in the skin dermis and epidermis.[41,42] To understand which gene(s) may mediate the effect of 3D-GF-PADM on HSFs, we examined the expression of these three genes before and after 3D-GF-PADM treatment. We found that the expression of HAS2 was significantly elevated by 3D-GF-PADM treatment, while the expression of HAS1 and

Table 2 The primers used in this study

Target gene	Forward primer sequence (5′–3′)	Reverse primer sequence (5′–3′)
HAS1	GGAATAACCTCTTGCAGCAGTTTC	GCCGGTCATCCCCAAAAG
HAS2	GGGGGAGATGTCCAGATTTT	ATGCACTGAACACACCCAAA
HAS3	TATACCGCGCGCTCCAA	GCCACTCCCGGAAGTAAGACT
MMP-9	ACGATGACGAGTTGTGGTCC	TCGCTGGTACAGGTCGAGTA
GAPDH	GGCAAGTTCAACGGCACAGT	TGGTGAAGACGCCAGTAGACTC

HAS2 did not change substantially (Fig. 5E–G). This suggests that the 3D-GF-PADM upregulates HAS2 expression, which then increases the synthesis of hyaluronic acid. In addition, we found that the 3D-GF-PADM also upregulated COL I expression and the production of collagen (Fig. 5D and H), demonstrating that it possesses some properties similar to those of other skin fillers to promote collagen synthesis.

3.5. Signalling pathway underlying 3D-GF-PADM-induced hyaluronan production

We investigated the mechanism by which the 3D-GF-PADM upregulates HAS2 expression. It has been shown that multiple signalling pathways, including TGF-β/SMAD, PI3K/AKT, JAK2/STAT3 and MAPK/ERK, regulate HAS2 expression and hyaluronidase secretion. To determine whether any of these pathways mediates the upregulation of HAS2 expression by 3D-GF-PADM, we studied the effects of inhibitors specific to individual signalling pathways on HAS2 expression. The results showed that AG490 abolished HAS2 upregulated expression by 3D-GF-PADM, while the other inhibitors had little or no effect on HAS2 expression (Fig. 6A). Because AG490 is an inhibitor specific to JAK2/STAT3, this demonstrated that the JAK2/STAT3 signalling pathway mediates 3D-GF-PADM-induced HAS2 upregulation. To further confirm the role of the JAK2/STAT3 signalling pathway in this process, other components in this pathway were studied. The results showed that 3D-GF-PADM treatment increased the phosphorylation of JAK2 and STAT3, which eventually resulted in the elevated level of HAS2 protein. By contrast, AG490 significantly inhibited the phosphorylation of JAK2 and STAT3 (Fig. 6B and ESI Fig. 4†). These results are also consistent with our confocal microscopy observations, which showed upregulated HAS2 expression after 3D-GF-PADM treatment; moreover, such HAS2 upregulation was significantly inhibited by AG490 (Fig. 6C). It is thus clear that the 3D-GF-PADM upregulates HAS2 expression by activating the JAK2/STAT3 signalling pathway. Taking these findings together, we concluded that the mechanism underlying 3D-GF-PADM-induced hyaluronan secretion involves the following: 3D-GF-PADM treatment increases the level of JAK2 phosphorylation, which leads to the increased expression of STAT3; activated STAT3 then enters the nucleus and binds to the promoter of the HAS2 gene to upregulate its expression at both RNA and protein levels. This eventually results in an increase in the synthesis of hyaluronic acid (Fig. 7).

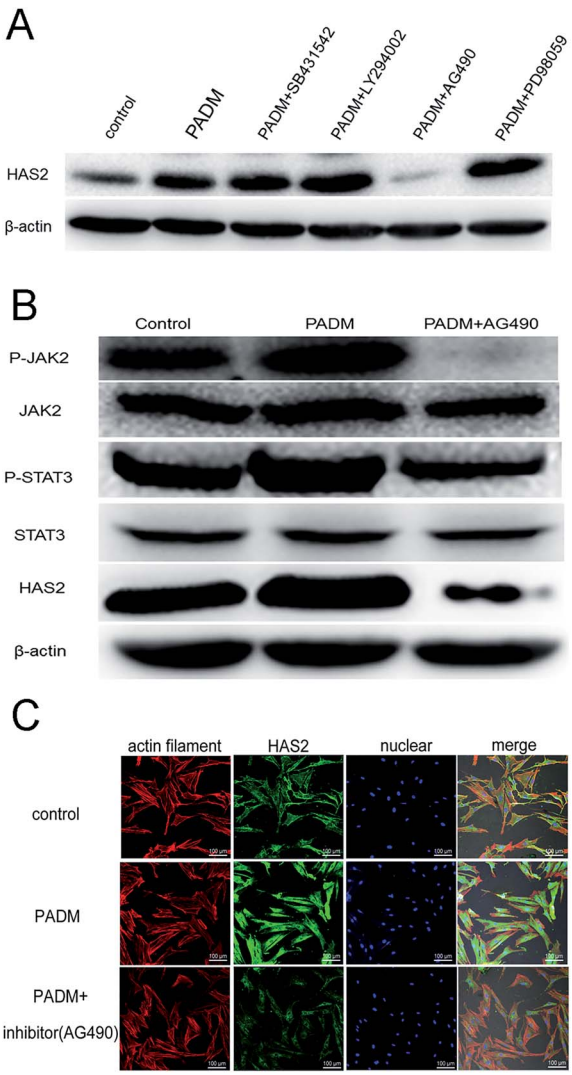

Fig. 6 (A) HAS2 expression can be inhibited by blocking the JAK2/STAT3 pathway in HSFs. HSFs were grown to 70–80% confluence and treated with 3D-GF-PADM alone or with the following pathway inhibitors: 10 μM TGF-β receptor inhibitor SB431542, 10 μM PI3K inhibitor LY294002, 10 μM JAK-2 inhibitor AG490, and 10 μM ERK-specific inhibitor PD98059. Cells were then lysed at 24 h after treatment and western blot analysis was performed for HAS2. (B) Inhibition of the JAK2/STAT3 signalling attenuates 3D-GF-PADM-induced HAS2 expression in HSFs. (C) Immunofluorescent staining of the 3D-GF-PADM.

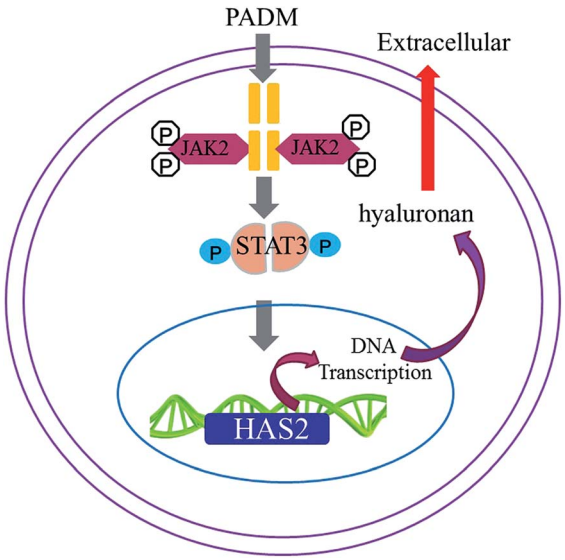

Fig. 7 The mechanism underlying 3D-GF-PADM-induced hyaluronan secretion. 3D-GF-PADM treatment increases the level of JAK2 phosphorylation, which leads to the increased expression of STAT3, and activated STAT3 enters the nucleus and binds to the promoter of the HAS2 gene to upregulate its expression at both RNA and protein levels. This eventually results in an increase in the synthesis of hyaluronic acid.

3.6. Long-term effects of 3D-GF-PADM *in vivo*

An *in vivo* experiment was performed to evaluate the long-term effects and inflammatory response of 3D-GF-PADM. Only a small number of mononuclear cells were found at the injection site at the early stage (1 week; ESI Fig. 5B†). Over time, these inflammatory cells disappeared, while fibroblasts colonised the injection area and secreted new collagen (1 and 3 months; ESI Fig. 5C and D†). These results demonstrate that there was no acute or delayed inflammatory reaction; more importantly, they show that 3D-GF-PADM exhibited high biocompatibility.

4. Conclusions

3D-GF-PADM possesses a complete three-dimensional structure and large amounts of proline, hydroxyproline and growth factors. Our data showed that this 3D-GF-PADM efficiently induces the secretion of hyaluronic acid from human skin fibroblasts by activating the JAK2/STAT3 signalling pathway. This indicates that 3D-GF-PADM can maintain a cosmetic filling effect for a long period. Our study has established a scientific foundation for developing a skin physical filler with the ability to effectively induce hyaluronic acid.

Ethical statement

All animal procedures were performed in accordance with the Guidelines for Care and Use of Laboratory Animals of Shanghai Jiao Tong University, and approved by the Animal Ethics Committee of Shanghai Ninth People's Hospital, affiliated with the School of Medicine, Shanghai Jiao Tong University.

Conflicts of interest

There are no conflicts to declare.

Acknowledgements

The authors are grateful to Yingen Pan, Jiangsu Unitrump BioMedical Technology Co., Ltd. (Nanjing, China), for technical advice and providing the 3D-GF-PADM. This work was supported by grants from the National Key Research and Development Program of China (2018YFC1105202), National Natural Science Foundation of China (No. 31600760), National Natural Science Foundation of China (No. 31470917), and Science and Technology Commission of Shanghai Municipality (18DZ22903000).

References

1 A. Adrien, A. Bonnet, D. Dufour, S. Baudouin, T. Maugard and N. Bridiau, *Carbohydr. Polym.*, 2017, **157**, 1306–1314.
2 U. Wollina and A. Goldman, *Clin. Dermatol.*, 2013, **31**(6), 731–736.
3 Y. Li, H. Cai, W. Fang, Q. Meng, Y. Wu, J. Li, M. Deng and X. Long, *Cells Tissues Organs*, 2014, **199**(2–3), 150–158.
4 G. Chow, J. Tauler and J. L. Mulshine, *J. Biomed. Biotechnol.*, 2010, **2010**, 485468.
5 J. J. Ross and R. T. Tranquillo, *Matrix Biol.*, 2003, **22**(6), 477–490.
6 Y. Zhou, Z. Yan, H. Zhang, W. Lu, S. Liu, X. Huang, H. Luo and Y. Jin, *Tissue Eng., Part A*, 2011, **17**(23–24), 2981–2997.
7 X. Zhang, Z. Deng, H. Wang, Z. Yang, W. Guo, Y. Li, D. Ma, C. Yu, Y. Zhang and Y. Jin, *Biomaterials*, 2009, **30**(14), 2666–2674.
8 C. M. Magin, D. L. Alge and K. S. Anseth, *Biomed. Mater.*, 2016, **11**(2), 022001.
9 A. Shimizu, D. P. Zankov, M. Kurokawa-Seo and H. Ogita, *Int. J. Mol. Sci.*, 2018, **19**(4), E1203.
10 Ł. A. Poniatowski, P. Wojdasiewicz, R. Gasik and D. Szukiewicz, *Mediators Inflammation*, 2015, **2015**, 137823.
11 C. M. Murphy, M. G. Haugh and F. J. O'Brien, *Biomaterials*, 2010, **31**(3), 461–466.
12 J. Kablik, G. D. Monheit, L. Yu, G. Chang and J. Gershkovich, *Dermatol. Surg.*, 2009, **35**(Suppl 1), 302–312.
13 Y. Murawaki, M. Koda, S. Yamada, H. Kawasaki, H. Shima and H. Burkhardt, *J. Hepatol.*, 1993, **18**(3), 328–334.
14 R. Osmers, H. Tschesche, W. Rath, M. Szeverényi, V. Süwer, I. Wölker and W. Kuhn, *Eur. J. Obstet. Gynecol. Reprod. Biol.*, 1994, **53**(1), 55–57.
15 U. Galili, *Biochimie*, 2001, **83**(7), 557–563.
16 H. J. Choi, M. K. Kim, H. J. Lee, S. H. Jeong, H. J. Kang, C. S. Park, C. G. Park, S. Joon Kim and W. R. Wee, *Xenotransplantation*, 2011, **18**(3), 176–182.
17 A. Alqahtani, M. Altuwaijri, A. Haddad, S. Al-johani, A. Al-qouzi, F. Aldugaishm, H. Heena, D. Jawdat and R. M. Kana, *Int. J. Biol. Biomed.*, 2018, **3**, 22–25.
18 G. F. Muti, *J. Drugs Dermatol.*, 2019, **18**, 86–91.
19 M. J. Ban, J. H. Park, J. W. Kim, K. N. Park, J. Y. Lee, H. K. Kim and S. W. Lee, *Clin. Exp. Otorhinolaryngol.*, 2017, **10**(4), 349–356.
20 T. Lin and L. Gong, *Drug Des., Dev. Ther.*, 2017, **11**, 1147–1158.
21 A. D. Theocharis, S. S. Skandalis, C. Gialeli and N. K. Karamanos, *Adv. Drug Deliv. Rev.*, 2016, **97**, 4–27.
22 N. A. Afratis and I. Sagi, *Methods Mol. Biol.*, 2019, **1952**, 261–275.
23 T. J. Keane and S. F. Badylak, *J. Tissue Eng. Regener. Med.*, 2015, **9**(5), 504–511.
24 E. S. Wijelath, S. Rahman, M. Namekata, J. Murray, T. Nishimura, Z. Mostafavi-Pour, Y. Patel, Y. Suda, M. J. Humphries and M. Sobel, *Circ. Res.*, 2006, **99**(8), 853–860.
25 S. Rahman, Y. Patel, J. Murray, K. V. Patel, R. Sumathipala, M. Sobel and E. S. Wijelath, *BMC Cell Biol.*, 2005, **6**(1), 8.
26 R. Goetz and M. Mohammadi, *Nat. Rev. Mol. Cell Biol.*, 2013, **14**(3), 166–180.
27 R. J. Walter, T. Matsuda, H. M. Reyes, J. M. Walter and M. Hanumadass, *Burns*, 1998, **24**(2), 104–113.
28 J. Y. Won, M. H. Lee, M. J. Kim, K. H. Min, G. Ahn, J. S. Han, S. Jin, W. S. Yun and J. H. Shim, *Artif. Cells, Nanomed., Biotechnol.*, 2019, **47**(1), 644–649.
29 L. J. Ning, Y. L. Jiang, C. H. Zhang, Y. Zhang, J. L. Yang, J. Cui, Y. J. Zhang, X. Yao, J. C. Luo and T. W. Qin, *J. Biomed. Mater. Res., Part A*, 2017, **105**(8), 2299–2311.

30 M. He, A. Callanan, K. Lagaras, J. A. M. Steele and M. M. Stevens, *J. Biomed. Mater. Res., Part B*, 2017, **105**(6), 1352–1360.
31 Y. Wang, J. Bao, X. Wu, Q. Wu, Y. Li, Y. Zhou, L. Li and H. Bu, *Sci. Rep.*, 2016, **6**, 24779.
32 S. Gobinathan, S. S. Zainol, S. F. Azizi, N. M. Iman, R. Muniandy, H. N. Hasmad, M. R. B. Yusof, S. Husain, H. Abd Aziz and Y. Lokanathan, *J. Biomater. Sci., Polym. Ed.*, 2018, **29**(17), 2051–2067.
33 T. Fujiwara, D. Duscher, K. C. Rustad, R. Kosaraju, M. Rodrigues, A. J. Whittam, M. Januszyk, Z. N. Maan and G. C. Gurtner, *Exp. Dermatol.*, 2016, **25**(3), 206–211.
34 L. Ge, S. Zheng and H. Wei, *Burns*, 2009, **35**(1), 46–50.
35 B. Schönmeyr, N. Clavin, T. Avraham, V. Longo and B. J. Mehrara, *Tissue Eng., Part A*, 2009, **15**(7), 1833–1841.
36 H. Ohara, S. Ichikawa, H. Matsumoto, M. Akiyama, N. Fujimoto, T. Kobayashi and S. Tajima, *J. Dermatol.*, 2010, **37**(4), 330–338.
37 P. Heldin, T. C. Laurent and C. H. Heldin, *Biochem. J.*, 1989, **258**(3), 919–922.
38 S. M. Mârza, K. Magyari, S. Bogdan, M. Moldovan, C. Peștean, A. Nagy, F. Tăbăran, E. Licarete, S. Suarasan, A. Dreanca, L. Baia and I. Papuc, *Biomed. Mater.*, 2019, **14**(2), 025011.
39 L. Ravanti and V. M. Kähäri, *Int. J. Mol. Med.*, 2000, **6**(4), 391–407.
40 J. J. Nordlund, *Dermatol. Clin.*, 2007, **25**(3), 271–281.
41 T. Sayo, Y. Sugiyama, Y. Takahashi, N. Ozawa, S. Sakai, O. Ishikawa, M. Tamura and S. Inoue, *J. Invest. Dermatol.*, 2002, **118**(1), 43–48.
42 Y. Yamada, N. Itano, K. Hata, M. Ueda and K. Kimata, *J. Invest. Dermatol.*, 2004, **122**(3), 631–639.